Correction for Patient and Organ Movement in SPECT: Application to Exercise Thallium-201 Cardiac Imaging

William J. Geckle, Terry L. Frank, Jonathan M. Links, and Lewis C. Becker

Divisions of Cardiology and Nuclear Medicine, Departments of Medicine and Radiology, The Johns Hopkins Medical Institutions, and the Johns Hopkins University Applied Physics Laboratory, Baltimore, Maryland

We describe a technique for correction of artifacts in exercise ^{201}Tl single photon emission computed tomography (SPECT) images arising from abrupt or gradual translational movement of the heart during acquisition. The procedure involves the tracking of the "center of the heart" in serial projection images using an algorithm which we call "diverging squares". Each projection image is then realigned in the x-y plane so that the heart center conforms to the projected position of a fixed point in space. The shifted projections are reconstructed using the normal filtered backprojection algorithm. In validation studies, the motion correction procedure successfully eliminated movement artifacts in a heart phantom. Image quality was also improved in over one-half of 36 exercise thallium patient studies. The corrected images had smoother and more continuous left ventricular walls, greater clarity of the left ventricular cavity, and reduced streak artifacts. Rest injected or redistribution images, however, were often made worse, due to reduced heart to liver activity ratios and poor tracking of the heart center. Analysis of curves of heart position versus projection angle suggests that translation of the heart is common during imaging after exercise, and results from both abrupt patient movements, and a gradual upward shift of the heart. Our motion correction technique appears to represent a promising new approach for elimination of movement artifacts and enhancement of resolution in exercise ^{201}Tl cardiac SPECT images.

J Nucl Med 29:441–450, 1988

Thallium-201 (^{201}Tl) single photon emission computed tomography (SPECT) has been shown to be valuable for assessing regional myocardial perfusion in patients with known or suspected coronary artery disease (*1–8*). Increasingly, thallium SPECT has been found to be superior to standard planar imaging, with improved lesion contrast and spatial localization, and fewer chest wall attenuation artifacts (*1–6*). However, SPECT may be associated with significant reconstruction artifacts, and system performance may be limited by errors in the acquired emission data which are propagated through the reconstruction process (*9,10*). A contributing factor to the loss of image quality in perfusion studies may be a shift in heart position within the thorax during acquisition, due to voluntary or involuntary patient movement, or changes in central blood volume or lung volume. The effect of organ movement is to misalign the projection images and introduce an unmodeled blur function into the reconstruction, leading to the loss of resolution and introduction of image artifacts.

Image degradation due to changing heart position has been documented (*11,12*) and voluntary patient motion artifacts have been simulated and described (*13*). In addition, a gradual upward shift in the position of the heart has been described following cessation of vigorous exercise, termed "upward creep" (*14*), which results in artifactual perfusion defects in the inferior left ventricular wall. Although the problems created by heart movement are well understood, no procedure to correct the error has been published.

In this report we describe a technique to correct for the average shift in heart position occurring between projection images by appropriately realigning each of the 60 images contained in a 180-degree acquisition.

Received Dec. 22, 1986; revision accepted Oct. 9, 1987.

For reprints contact: Lewis C. Becker, MD, Johns Hopkins Medical Institutions, Halsted 500, 600 N. Wolfe St., Baltimore, MD 21205.

This paper describes the algorithms and techniques involved in heart movement correction and presents an initial evaluation of its performance in phantoms and patients.

MATERIALS AND METHODS

Overview

The correction procedure begins by locating the position of the heart in each projection image. The "center of the heart" is defined as the center of a standardized square region that is roughly the size of an average emission projection image of the heart. Every projection image is then shifted prior to reconstruction, such that the heart location in the shifted image corresponds to the projected location of an arbitrary *fixed* point in space.

Object Tracking

In order to successfully align the projection images, the position of the "center of the heart" must be identified and located in each projection image. In initial attempts, a gamma emitting marker was attached to the patient's thorax in various positions, including the suprasternal notch, left supraclavicular area, left mid-axillary line, xiphoid, and upper and lower thoracic spine, in an effort to locate an external reference point that would move consistently with the heart. Although external markers accurately reflected gross patient motion in the axis of, and perpendicular to the axis of, the table, they did not track the "upward creep" motion of the heart, nor did they consistently move with the heart as the left arm was raised above the head to allow passage of the camera head close to the thorax. Thus, although external markers have been successfully employed for planar exercise scintigraphic studies (*15*), they do not appear to be applicable to tomographic systems.

In the technique we have developed, the heart itself is followed in each projection using a modification of the "converging squares" algorithm (*16*), which we call "diverging squares". It is used to identify and track that square region of the image containing the most counts, the center of which is defined as the "center of the heart". The first step in the diverging squares algorithm is to interactively position a 10 × 10 pixel square (3 mm/pixel) over the interior of the left ventricle (the chamber) in the first projection image. The algorithm then proceeds to form four 11 × 11 pixel squares, each of which contains the initial 10 × 10 square plus one of the four possible adjacent row-column pairs (Fig. 1). That 11 × 11 square (of the four) with the highest total counts is chosen, and four 12 × 12 pixel squares are formed, each of which contains the chosen 11 × 11 pixel square plus an additional adjacent row-column pair. That 12 × 12 square (of the four) with the highest total counts is chosen, and the process is repeated until the square is expanded to a size of 20 × 20 pixels, a size which we found encompasses most of the left ventricular myocardium in an average patient. The center of this final 20 × 20 pixel square is considered the "center of the heart" in the first projection. For the successive projections, the algorithm begins by centering the initial 10 × 10 pixel square on the previous projection's "heart center", and proceeds in the same manner as described above to expand the square to a size of 20 × 20 pixels.

Projection Alignment

The alignment algorithm shifts the position of the heart in each projection image such that the center of the heart follows the projection trajectory of an off-axis, fixed point in space (sinusoidal motion in the x dimension and a straight line in the z dimension). For the geometry illustrated in Figure 2, the location in image coordinates (x_i, y_i) of the projection of a point located at (x, y, z) can be shown by simple geometry to be

$$x_i = A \sin(\theta - \omega)$$

$$y_i = z$$

where

$\omega = \tan^{-1}(y/x)$ and

θ = camera angle and

$A = (x^2 + y^2)^{1/2}$

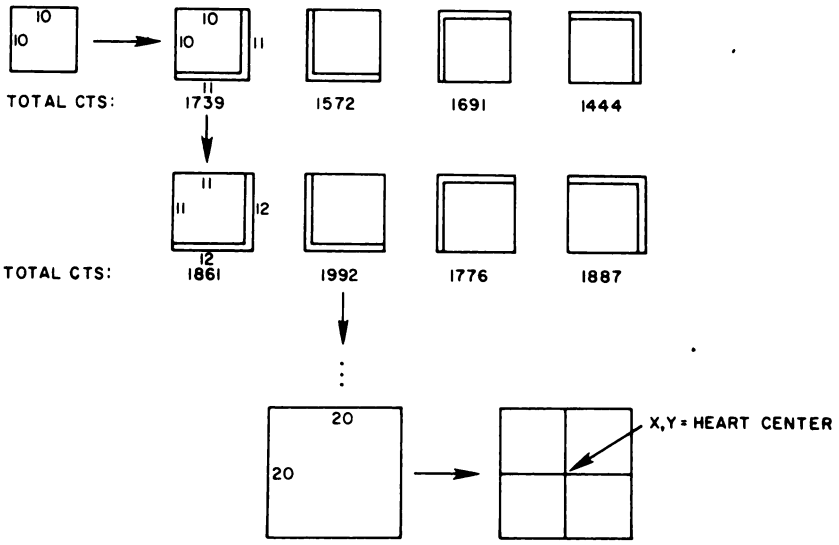

FIGURE 1
Illustration of diverging squares algorithm used to track the heart center. Initially, a 10 × 10 pixel box is placed within the heart. By annexing one adjacent row and column, the box is expanded to produce four 11 × 11 pixel squares. The one containing the highest counts is chosen and further expanded by adding one adjacent row and column to form four 12 × 12 pixel squares. The process is repeated until the square reaches a size of 20 × 20 pixels; the center is defined as the "heart center" and is used to position the initial 10 × 10 pixel box in the next projection image. The counts shown are representative of the values found in our studies but do not come from one specific study.

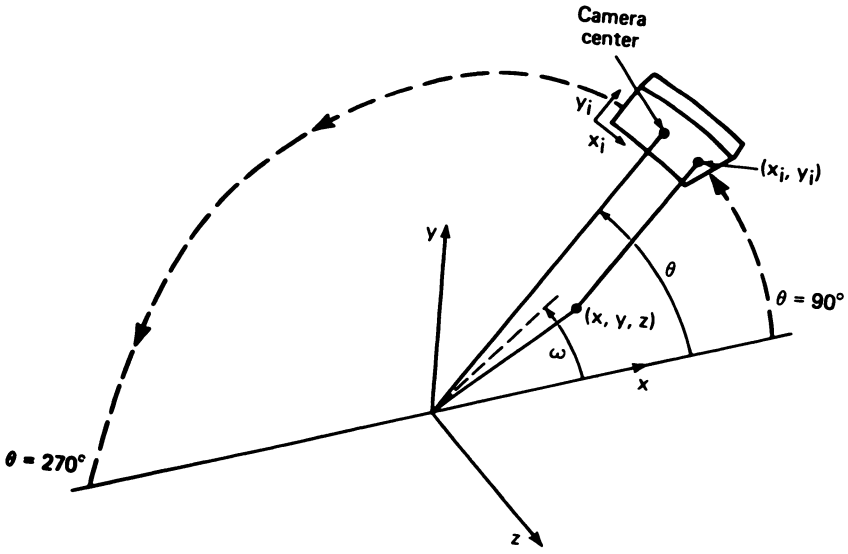

FIGURE 2
Diagram showing the relations between center of rotation (origin), camera head undergoing counterclockwise circular orbit at projection angle θ, and offset fixed point in space with three-space coordinates x, y, z and projected image coordinates x_i, y_i. In our imaging system, $\theta = 0$ is defined as vertically downwards. The dashed line at angle represents the projection on the x-y plane of the chord connecting the origin and x, y, z. See text for details.

These equations assume that the origin is at the axis of rotation of the camera gantry. For a fixed point in space, therefore, the location of the projection of that point in an acquired, raw projection image is uniquely determined.

The selection of values for the parameters A and ω, as defined above, is arbitrary for the filtered back-projection parallel beam data used here. The projection images may be shifted to positions corresponding to any fixed point using the equations above, as long as the original relative angular dependence of the projections is preserved. The location of the heart within the reconstructed image varies with the choice of different fixed point projection trajectories. Values of $A = \omega = 0$, for example, would result in the heart appearing in the center of the image, which represents the center of rotation. A determines the distance of the heart from the center of the reconstruction matrix, while ω affects its angular position in the matrix.

For convenience, we chose values for A and ω based on typical heart locations in patient studies (A = 25 pixels, or 7.5 cm, off the axis of rotation; $\omega = 0$). Each projection image was first shifted in the x-direction so that the x-coordinate of the heart center conformed to the relation $x_i = 25 (\sin \theta) +$ AOR, where θ begins at 140° (the first projection angle) and increases 3° for each successive projection image, and AOR represents the axis of rotation. The AOR x-offset, which is determined by a line source calibration study, is required in the equation because in our implementation, the origin is in the lower left hand corner of the matrix rather than at the actual AOR. Each image was then shifted in the y-direction, to align the y-coordinate of the heart center with the y-value determined in the first projection image.

Phantom Studies

To assess the ability of the motion correction program to improve image quality of commercially available SPECT phantom was used with a heart insert oriented approximately 45° off the longitudinal axis (Data Spectrum Corporation). The outer chamber of the insert, simulating the myocardium, was filled with thallous-201 chloride, 2 μCi/ml, and a capillary tube containing the same concentration of tracer was attached to the outside of the phantom along the longitudinal axis. The phantom was filled with nonradioactive water. Using a large field of view tomographic camera (Technicare Omega 500, Technicare, Solon, OH) fitted with a general-all-purpose, parallel hole collimator, and interfaced with a Technicare 560 computer, projection images (128 × 128) were obtained every 3° over 180° from 40° "right anterior oblique" (defined as "140°" in our system) to 50° "left posterior oblique" (defined as "320°") with 1.4× camera magnification. Raw images were corrected by a 128 million count flood field, and 3 pixel (9 mm) thick transaxial images were obtained by reconstruction using a filtered backprojection algorithm (Hanning filter with an 0.30 cutoff or Shepp-Logan filter with a cutoff of 0.70).

Two additional studies were acquired to simulate heart motion. For transaxial motion, the ECT table, including phantom and capillary tube, was moved sideways approximately 2.5 cm at image number 17, corresponding to a 10° left anterior oblique projection. To simulate axial motion, the table was moved upwards 2.5 cm at image number 17. Transaxial images were reconstructed with and without application of the heart tracking and projection alignment algorithms described above, and for each study the three image sets—original acquisition, motion without correction, and motion with correction—were compared. To more quantitatively assess the effects of motion correction, profiles were constructed through the cross-sectional images of the capillary tube, and the full width at half maximum (FWHM) was determined.

Patient Studies

Standard exercise ^{201}Tl tomographic images were obtained in 36 subjects using the same camera/collimator system described above. Eleven subjects were normal volunteers, 14 were asymptomatic siblings of patients with premature coronary artery disease (ten of the siblings had undergone coronary arteriography), and 11 were symptomatic patients being evaluated for coronary artery disease (eight with coronary arteriography). Projection images were acquired every 3° over 180°, 30 sec per view, as in the phantom studies. The radius of rotation was as small as possible, averaging ~20 cm. Transaxial slices (3 pixels thick) were reconstructed by filtered backprojection (Hanning 0.30 filter). Attenuation correction was not performed. The transaxial data were then reoriented

around the true cardiac longitudinal axis to form short axis and vertical long axis image sets.

To compare motion-corrected and nonmotion-corrected images for each patient, the projection data were reconstructed again following application of the motion correction algorithm described above. For each of the three orientations (transaxial, short axis, and long axis), eight slices from the standard image set were displayed side by side with the corresponding eight slices from the motion-corrected study. The image sets were displayed in random order on the video monitor and viewed by three experienced observers who were blinded as to which image set was standard and which was motion corrected. Image quality was assessed visually according to the smoothness and continuity of myocardial walls, clarity of the left ventricular cavity, and absence of streak artifacts. Paired image sets were compared to determine whether one of the two studies was "much better", "somewhat better", or "not significantly different" than the other. The code identifying which image set was motion corrected was broken only after all of the patients had been analyzed.

To determine the ability of the motion correction program to work successfully under conditions of reduced total counts and heart/background ratio, ten redistribution studies and ten rest injected thallium tomographic studies were motion corrected and compared with the standard image set.

To determine whether motion correction might artifactually eliminate exercise perfusion defects, particularly inferior ones, ten patients were randomly selected with known right and/or circumflex coronary artery disease and an inferior wall defect in the nonmotion corrected exercise study. The corrected and noncorrected image sets were displayed in random-order and compared.

RESULTS

Phantom Studies

The ability of the motion correction algorithm to eliminate transaxial and axial movement-related artifacts was evaluated in the SPECT heart phantom (Figs. 3 and 4). The first row in Figure 3, obtained without movement of the phantom, shows from left to right, a reconstructed cross-sectional slice through the capillary tube, a reconstructed slice through the simulated left ventricle, a "sinogram" through the capillary tube (obtained by vertically stacking the same one pixel thick horizontal row from each of the 60 successive projection images), and a sinogram-type display of the x-coordinate and y-coordinate of the computer-determined

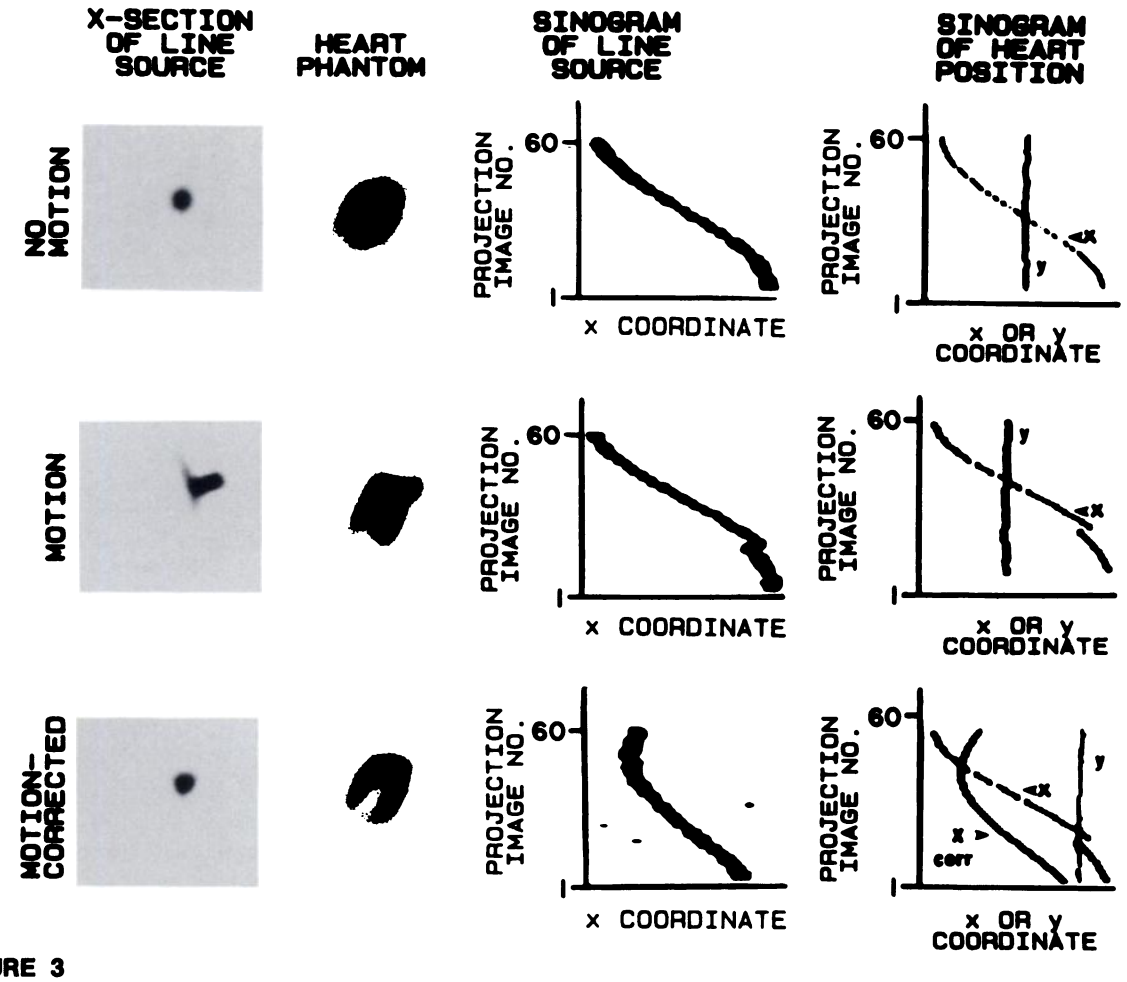

FIGURE 3
Heart phantom study: effect of transaxial (x-direction) movement. See text.

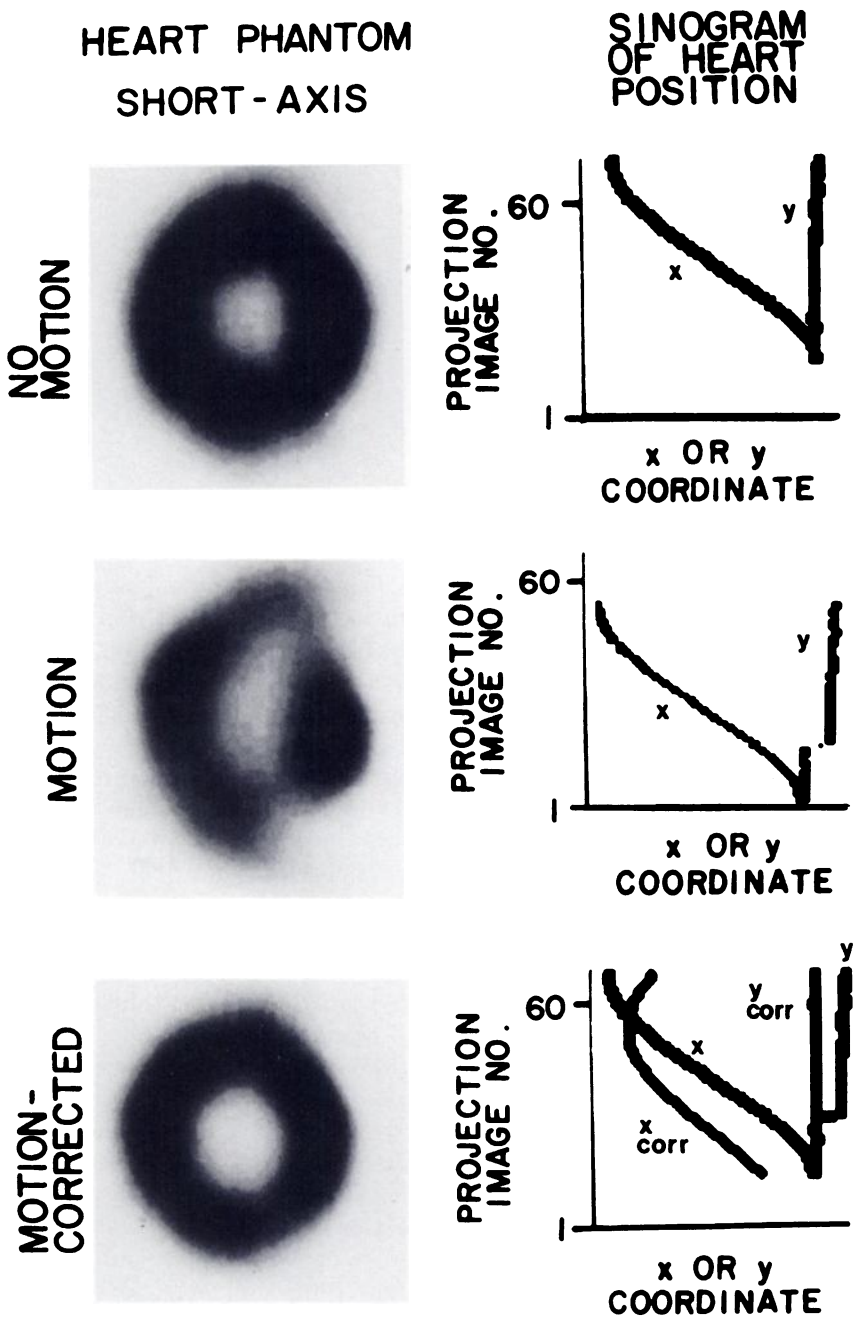

FIGURE 4
Heart phantom study: effect of 2.5 cm axial (y-direction) movement at projection image 17 on short axis tomogram, and correction by motion correction algorithm.

"center of the heart", presented as a stacked plot from the first to the last projection image. Note that the "left ventricular" image is smooth and free of artifacts, and that the derived x-coordinate curve of the "heart center" closely matches the sinogram through the capillary tube. The y-coordinate curve deviates by one pixel (3 mm) at some projection angles, despite the absence of real motion, possibly because of statistical noise or a change in the shape of the simulated left ventricle as the camera moves around the phantom. The middle row shows the effects of 2.5 cm of transverse (transaxial) motion applied at projection image number 17. The point source is blurred, the transaxial image of the "left ventricle" shows significant artifacts, including two hot areas, an apparent reduction of activity at the "apex", and a streak extending from the back of the "septum", and the sinogram shows an abrupt rightward movement about one third of the way up from the bottom, corresponding to the translational movement of the phantom. The heart-center tracking program successfully identifies the heart movement, with the x-coordinate curve precisely mirroring the capillary tube sinogram and the y-coordinate curve showing no significant change. The bottom row shows the results of motion correction. The point source is again sharp and round, the "left ventricle" is free of artifacts and the sinogram is again smooth. Each projection image has been realigned so that the "center of the heart" is shifted to an

arbitrary but fixed point in space, resulting in a sinogram of somewhat different amplitude and phase. The right panel shows the uncorrected and corrected x-coordinate curves of the heart center. The y-coordinate curve of the shifted data (not shown) is represented by a vertical line. Measurements of the FWHM for the point source obtained without motion, with motion, and after motion correction, are provided in Table 1.

Figure 4 shows the image degradation arising from axial movement of the heart phantom (2.5 cm at projection image number 17) and the improvement after motion correction. The sinograms show the tracked x and y positions of the heart center before and after image realignment.

To determine whether application of motion correction might cause artifactual defects in the heart phantom, the algorithm was applied to a normal data set that had been acquired without movement of the phantom. The reconstructed images appeared virtually identical to the non-motion corrected images.

Patient Studies

Motion correction provided an improvement in image quality in over half of the exercise studies examined in blinded readings (Table 2). In 25% of patients the motion corrected study was judged "much better" than the standard image set, while in an additional 28% it was judged "somewhat better". In only three patients (8%) was the motion corrected exercise study judged to be worse. A review of these three patients revealed the following: in one patient, heart tracking at the beginning and end of the acquisition was suboptimal due to low heart activity; the second patient, an asymptomatic sibling with a normal exercise test, had a streak artifact at the apex in the motion corrected study but also had more homogeneous uptake in the inferior wall (no reason could be ascertained for the streak artifact); the third patient had a very small difference between corrected and noncorrected studies and no cause could be found. Results of motion correction were similar in the normal volunteer, sibling, and clinical subject groups (Table 2).

Movement artifacts were most frequently related to either abrupt shifts in heart position as the left arm was raised above the head for close camera positioning, or to gradual "upward creep" in heart position during acquisition. Figure 5 illustrates significant image degradation in a sibling with a normal coronary arteriogram due to a sudden 1.8 cm upward movement of the heart (shift in y-coordinate of the heart center) as the left arm was repositioned. The transaxial view shows blurring of the left ventricular cavity and streak artifacts arising from the apex; the short axis view shows segmentation of myocardial activity, a "hot spot" in the lateral wall, and an apparent inferior wall perfusion defect; and the long axis view shows blurring and smudging of the inferior wall and a "hot spot" at the apex. After motion correction, the images are markedly improved with more homogeneous distribution of activity, greater clarity of the left ventricular cavity, and diminution of streak artifacts.

Figure 6 illustrates image degradation in another sibling with normal coronary arteries resulting from shifts in both x and y positions of the heart coincident with left arm repositioning. The y-coordinate curve shows an upward shift of 1.2 cm over about six projection angles, while the x-coordinate curve demonstrates a sudden shift to the left over two angles. The transaxial view shows prominent streak artifacts coming off the lateral wall, apex, and back of the septum, while the short axis view shows an apparent inferior wall perfusion defect. After motion correction, the streak artifacts are gone and the inferior wall "defect" is less apparent, although not completely gone. Attenuation effects may account for the remainder of the inferior wall artifact.

Figure 7 illustrates image artifacts in a normal volunteer subject caused by "upward creep", gradual upward displacement of the heart (change in y-coordinate) without any abrupt translational shifts. The transaxial view shows a hot spot at the junction of the right and left ventricles; the short axis view shows hot spots in the lateral and anterior walls, a distortion of left ventricular shape, segmentation of the left ventricle, and moderate streak artifacts; the long axis view shows a very prominent artifact resembling an extra ventricular wall with decreased uptake in the inferior region. After motion correction the left ventricular activity is homogeneous and the "extra wall" has disappeared.

TABLE 1
Phantom Study: FWHM of Cross-Section Through Line Source

	Reconstruction filter	
	Hanning 0.30	Shepp-Logan 0.70
No motion	2.41 cm	1.22 cm
Motion	4.20 cm	2.41 cm
Motion corrected	2.47 cm	1.58 cm

TABLE 2
Motion-Corrected Compared with Uncorrected Exercise Studies

	Much better	Somewhat better	No difference	Somewhat worse	Much worse
Normal volunteers (n = 11)	1	4	6	0	0
Siblings (n = 14)	5	4	3	2	0
Clinical (n = 11)	3	2	5	1	0
Total (n = 36)	9 (25%)	10 (28%)	14 (39%)	3 (8%)	0 (0%)

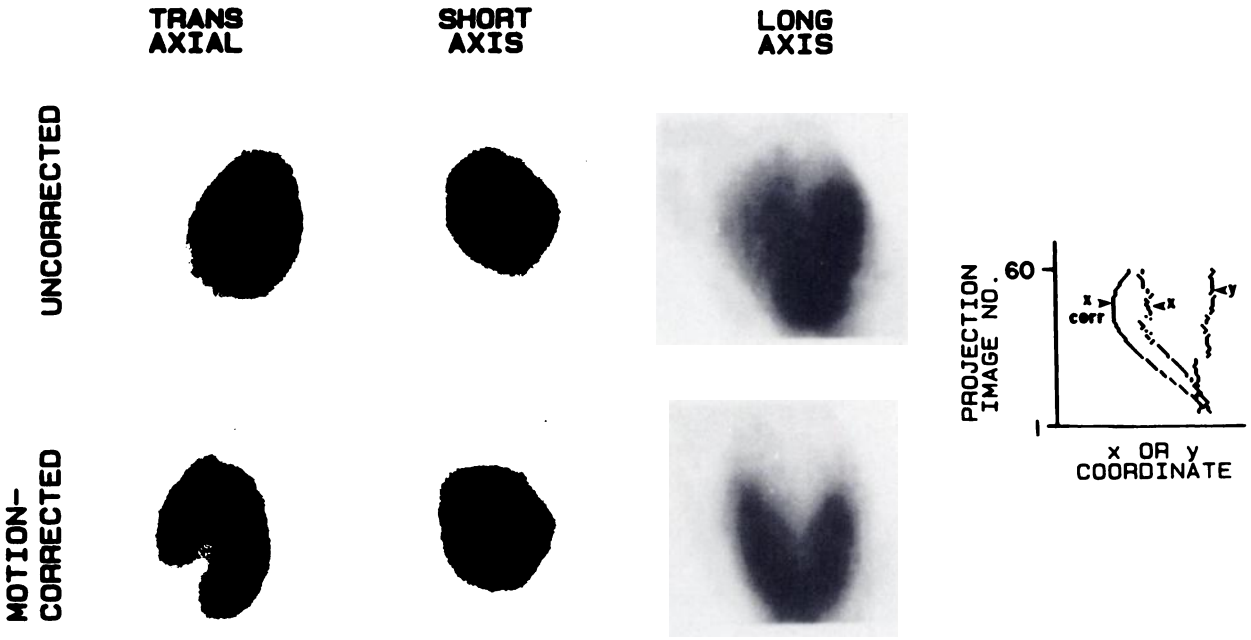

FIGURE 5
Exercise images from a patient with normal coronary arteriogram. Uncorrected images show artifactual inferior wall perfusion defect which disappears after motion correction. Sinogram display tracking the x- and y-coordinates of the heart center indicates a sudden upward shift in heart position about one-third of the way through acquisition, probably related to raising of left arm over head. See text.

Since motion correction appeared to make the inferior wall in particular more homogeneous, we compared corrected and uncorrected exercise studies from ten patients with known right and/or circumflex coronary artery disease to evaluate the possibility that motion correction might "blur" inferior wall perfusion defects. On a scale of 0 (no defect) to +++ (severe defect), the number of patients with inferior wall defects

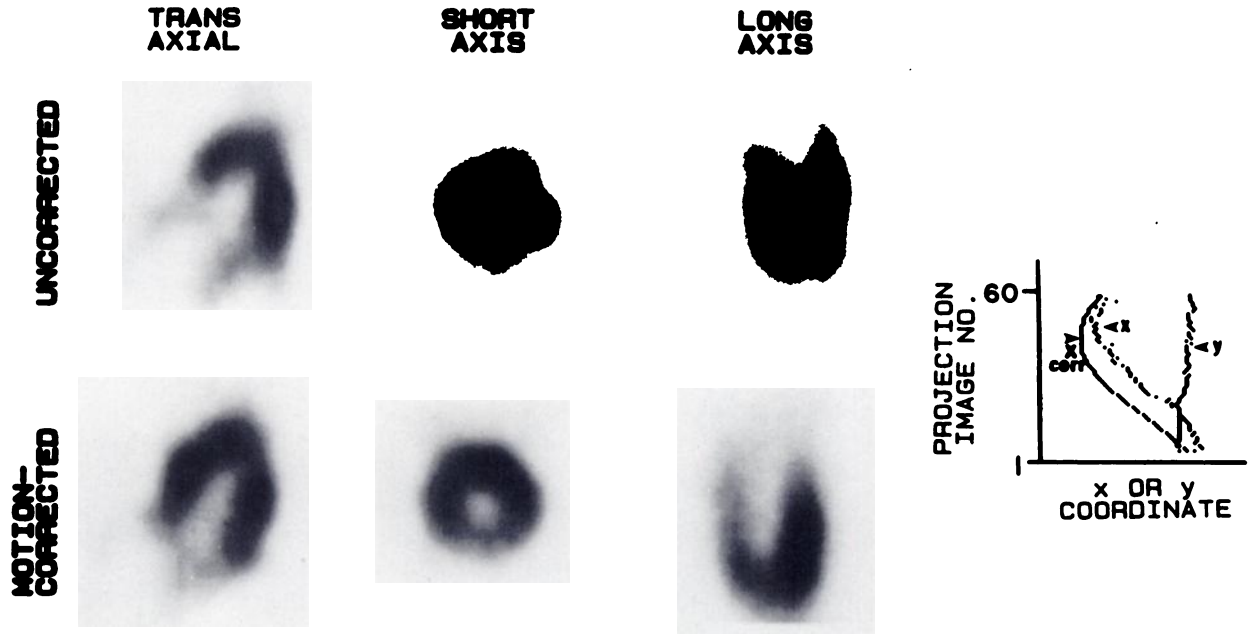

FIGURE 6
Exercise images from a second patient with normal coronary arteriogram. Uncorrected images show artifactual inferior wall perfusion defect related to shifts in both the x- and y-coordinates of the heart center. Corrected image set is significantly improved. See text.

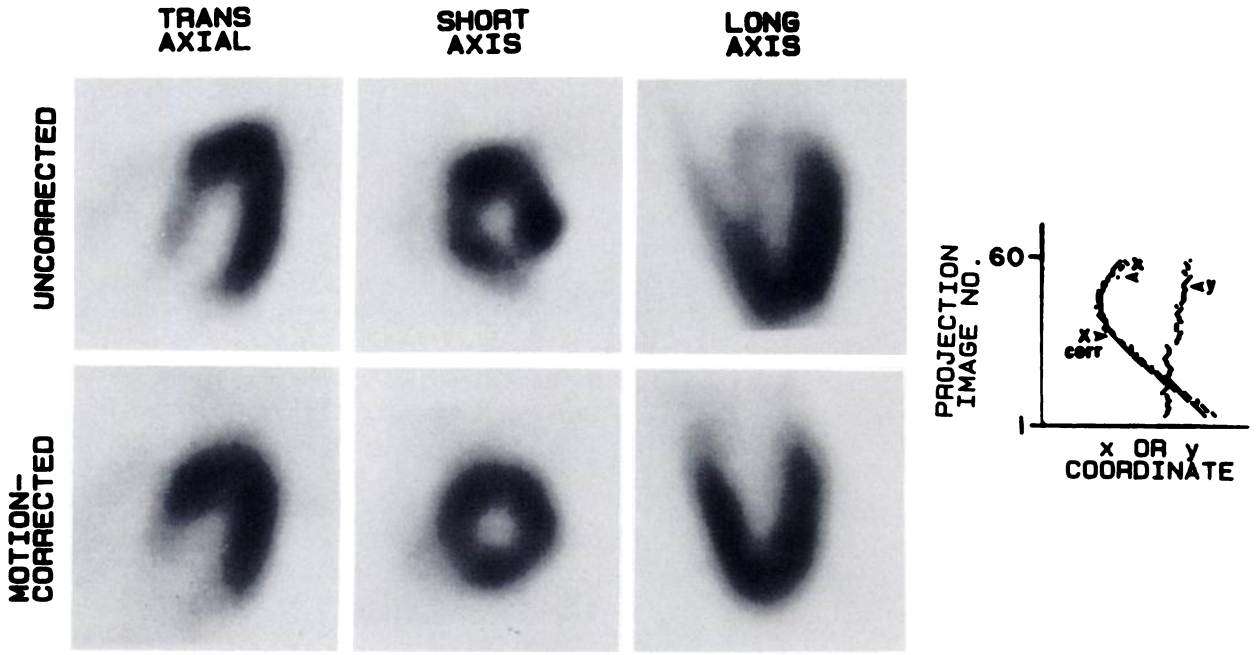

FIGURE 7
Exercise images from a normal volunteer with a normal stress test. Artifactual "extra wall" is seen in uncorrected image set related to gradual "upward creep" of heart. Corrected images are markedly improved. See text.

were as follows: 3 with +++, 4 with ++, 1 with +, 1 with ±, 1 with 0. In each patient the reading on the motion corrected study was identical.

Although results were good with correction of exercise studies, the same could not be said for redistribution or rest-injected studies. Blinded visual comparison of ten redistribution studies showed that the motion-corrected images were "much better" than the uncorrected images in two patients, "somewhat better" in two, "no different" in three, "somewhat worse" in two, and "much worse" in one. For the ten rest studies, the motion corrected images were judged to be "no different" in three, "somewhat worse" in five, and "much worse" in two. Worsening of the images after motion correction appeared to be related to poor tracking of the heart. Reduced heart to liver and heart to lung activities were sometimes associated with inaccurate localization of the heart center, leading to inappropriate realignment of projection images before reconstruction. Although heart activity was reduced ~50% in redistribution or rest-injected studies, the relation between accuracy of heart tracking and intensity of heart activity in the projection data was not a simple one. Heart activity in a 20 × 20 pixel box positioned over the heart averaged 9.47 counts/pixel for the three people in which motion correction degraded the reconstructed stress image (see above) compared to 10.16 counts/pixel for the three people illustrated in Figures 5–7 with marked image improvement. Activity in a 10-pixel-wide border around the heart was also similar, averaging 4.32 and 4.58 counts/pixel, respectively.

DISCUSSION

We have developed a technique for correction of motion artifacts in ^{201}Tl SPECT images arising from both patient motion and a gradual upward shift in heart position following exercise. Although others have described methods for *monitoring* the heart movement during acquisition of SPECT studies using summed projection images of the heart (*17*) or cross-correlation techniques (*18*), this study represents the first report of an automated method for correction of the artifacts produced by abrupt or gradual translational movements of the heart. The procedure involves the tracking of the "center of the heart" in serial projection images and realigning each projection image in the x-y plane so that the center conforms to an arbitrary but fixed point in space. The shifted projections are then backprojected in the normal manner. The procedure does not affect normal acquisition procedures and does not require the collection of any additional data. The software, written in BASIC, currently takes ~9 min to correct a full 60-image projection set on our tomographic system. Quantitative and qualitative phantom studies, as well as initial patient exercise studies, indicate a significant improvement in the overall quality of SPECT images following application of this correction.

We investigated several different methods of determining heart location. The "converging squares" intensity peak finding algorithm and centroid tracking methods were both implemented, but behaved poorly due to the influence of projected source activity external to the

heart (e.g., liver). A more successful approach, the "diverging squares" algorithm, was developed to automatically provide the heart position and avoid falsely tracking external uptake or noise regions. By initiating the tracking process within the heart and expanding to a final region size which is approximately that of the heart, noncardiac regions of uptake were found to have relatively little effect on the identification of the heart center. The procedure retains, however, the computational efficiencies inherent in the converging squares approach (*16*). In addition, the "diverging squares" algorithm is relatively insensitive to noise and requires no empirical parameters, such as threshold values or noise statistics.

Errors may nevertheless occur, even with the "diverging squares" algorithm, in projections where external regions of thallium uptake overlap the heart. Although this was not seen during our exercise patient studies, it was a significant problem in some rest-injected and redistribution thallium studies, which had relatively high liver uptake, and in some studies with severe defects in the inferior wall. Similarly, data derived from projection images with low heart uptake due to attenuation tended to be less accurate, since the diverging squares algorithm attempts to locate regions of high uptake relative to the surrounding background. The patient example in Figure 5 illustrates this point. The upper third of the x-coordinate curve is noisy, suggesting that the center of the heart was not being tracked precisely in the left posterior oblique positions (the most attenuated projections). Despite this problem, the motion-corrected images are markedly improved compared to the standard non-motion-corrected images. The effect of eliminating frames with poor heart to background definition from the raw projection data set prior to reconstruction is currently being investigated, since such frames provide little information on source activity and may, in fact, degrade overall spatial resolution.

Eisner et al. (*18,19*) have recently described a new technique for *detecting* (but not correcting) patient motion using frame-to-frame cross-correlation functions of the summed profiles in the vertical and horizontal directions of the planar projection images. Phantom studies showed that a 6-mm axial or transaxial movement could be easily detected. Like our diverging squares approach, this method can be automated and a hard copy output can be produced. However, errors may result from large abrupt motions disrupting the frame-to-frame correlation, or from poor target to background ratio. In addition, the cross-correlation approach does not detect a smooth continuous motion of the heart, as may occur during "upward creep" (*14*). We have found that this type of motion represents an important source of reconstruction artifact.

The alignment of projection images consists of shifting each projection image to provide a set of heart positions which follow the projected trajectory of a fixed point in space. As mentioned earlier, the choice of phase and amplitude for a particular sinusoid to model the projection shift is arbitrary, the only important constraint being that the sinusoid must be symmetric about the true axis of rotation of the camera. The amplitude of the sinusoid is related to the distance of the fixed point from the camera axis of rotation; to avoid the possibility of projection data being shifted so far that the heart falls partially outside of the image matrix, parameters were chosen so that the fixed point in space approximates the normal heart position in the thorax.

Misalignment in an uncorrected data set may also be related to factors other than patient or organ movement, such as center of rotation shifts with angle. Our procedure does not differentiate among the causes of misalignment, but globally corrects with a single correction shift. Thus, even in the absence of patient or organ movement, our procedure will shift the data to account for center of rotation errors. In our SPECT system, the manufacturer has implemented center of rotation correction as an integral part of the reconstruction procedure. Thus, the serial application of our movement correction and the manufacturer's center of rotation correction could result in over-correction. We routinely acquire a center of rotation phantom study for each patient, and examine the resulting correction factors, which represent horizontal shifts of the projection data. These shifts are always less than one pixel in magnitude. Since our movement correction procedure operates with whole pixel shifts, we have chosen not to disable the manufacturer's center of rotation correction. For those systems with larger center of rotation errors, and consequently larger correction shifts, the serial use of movement correction and center of rotation correction could result in artifacts. For those systems which implement center of rotation correction as a separate procedure whose output is a shifted set of projection data, there should be no problem as long as the center of rotation correction is performed before the movement correction procedure.

ACKNOWLEDGMENTS

This work was supported by a Specialized Center of Research in Ischemic Heart Disease Grant P50 HL 17655, from the National Institutes of Health, Bethesda, MD, and a gift from Mary L. Smith of the W. W. Smith Charitable Trust, Rosemont, PA. Dr. Becker was the recipient of a Frank T. McClure Fellowship in Cardiovascular Research from the Johns Hopkins Applied Physics Laboratory, Laurel, MD.

REFERENCES

1. Tamaki N, Mukai T, Ishu Y, et al. Clinical evaluation of thallium-201 emission myocardial tomography using a rotation gamma camera: comparison with seven-

pinhole tomography. *J Nucl Med* 1981; 22:849–855.
2. Maublant J, Cassagnes J, LeJeune JJ, et al. A comparison between conventional scintigraphy and emission tomography with thallium-201 in the detection of myocardial infarction: concise communication. *J Nucl Med* 1982; 23:204–208.
3. Ritchie JL, Williams DL, Harp G, et al. Transaxial tomography with thallium-201 for detecting remote myocardial infarction: comparison with planar imaging. *Am J Cardiol* 1982; 50:1236–1241.
4. Kirsch C-M, Doliwa R, Buell U, et al. Detection of severe coronary heart disease with Tl-201: comparison of resting single photon emission tomography with invasive arteriography. *J Nucl Med* 1983; 24:761–767.
5. Tamaki S, Kambara H, Kadota K, et al. Improved detection of myocardial infarction by emission computed tomography with thallium-201. Relation to infarct size. *Br Heart J* 1984; 5:621–627.
6. Fintel DJ, Links JM, Brinker JA, et al. Comparison of tomographic and planar thallium imaging for identification of disease in individual coronary arteries [Abstract]. *Circulation* 1985; (suppl III):III-137.
7. Prigent FM, Maddahi J, Garcia E, et al. Thallium-201 stress-redistribution myocardial rotational tomography: development of criteria for visual interpretation. *Am Heart J* 1985; 109:274–281.
8. Garcia EV, Van Train K, Maddahi J, et al. Quantification of rotational thallium-201 myocardial tomography. *J Nucl Med* 1985; 26:17–26.
9. Todd-Pokropek AE, Soussaline F. Quality control of SPECT systems: Removal of artifacts. *3rd World Conference of Nuclear Medicine and Biology.* Paris, 1982:1018–1021.
10. Todd-Pokropek AE. The mathematics and physics of ECT. In: Esser PD, ed. *Emission computed tomography: current trends.* New York: The Society of Nuclear Medicine, 1983.
11. Ter-Pogossian MM, Weiss ES, Coleman RE, et al. Computed tomography of the heart. *Am J Roentgenol* 1976; 127: 79–90.
12. Sagel SS, Weiss ES, Gillard RG, et al. Gated computed tomography of the human heart. *Invest Radiol* 1977; 12:563–566.
13. Yang C-K, Orphanoudakis SC, Strohbehn JW, et al. A simulation study of motion artifacts in computed tomography. *Phys Med Biol* 1982; 27:51–61.
14. Friedman J, Van Train K, Maddahi J, et al. "Upward creep" of the heart: a frequent source of false-positive reversible defects on Tl-201 stress-redistribution SPECT [Abstract]. *J Nucl Med* 1986; 27:899.
15. Groch MW, Erwin WD, Turner DA, et al. Dual-isotope motion correction technique for gated exercise scintigraphy. *J Nucl Med* 1985; 26:1478–1484.
16. O'Gorman L, Sanderson AC. The converging squares algorithm: an efficient method for locating peaks in multidimensions. *IEEE Trans Pattern Anal Mach Intell*, 1984; PAMI-7.
17. Freidman J, Garcia E, Berman D, et al. Motion detection and correction in Tl-201 SPECT imaging: A simple, practical method [Abstract]. *J Nucl Med* 1984; 25:70.
18. Eisner RL, Noever T, Nowak D, et al. Use of cross-correlation function to detect patient motion during SPECT imaging. *J Nucl Med* 1987; 28:97–101.
19. Eisner R, Churchwell A, Noever T, et al. Quantitative analysis of the tomographic Thallium-201 myocardial bullseye display: critical role of correcting for patient motion. *J Nucl Med* 1988; 29:91–97.